# 4

# Numerical Simulation of the Unsteady Shock Interaction of Blunt Body Flows

Leonid Bazyma[1], Vasyl Rashkovan[2] and Vladimir Golovanevskiy[3]
[1]*National Aerospace University "Kharkov Aviation Institute"*
[2]*National Polytechnic Institute*
[3]*Western Australian School of Mines, Curtin University*
[1]*Ukraine*
[2]*Mexico*
[3]*Australia*

## 1. Introduction

Supersonic and hypersonic space vehicles are extremely sensitive to aerodynamic resistance. The combination of the two main rocket operation factors, low altitude and high velocity, produces considerable heat flows in the stagnation region of the nose. For this reason, passive heat-transfer analysis under such conditions is very important for understanding and solving rocket operation problems.

The possibility of use of energy supply as the method of the overall control of the airflow is defined in the experimental and theoretical research (Adegren et al., 2001, 2005; Bazyma & Rashkovan, 2005; Tret'yakov et al., 1994, 1996). As an example, reduction of head resistance of a supersonic aircraft can be achieved with the introduction of energy into the contrary incoming flow. On the other hand, supply of energy may be used to minimize negative consequences of the shock-wave interaction when the streamlining of the aerodynamic configurations of the compound form occurs. For example, oblique shock waves, which are distributed from the bow part of an airplane or a rocket, can interact with a bow shock wave of any part of the fuselage construction (tail unit, suspension, hood, diffuser, etc.). In certain cases the shock-wave interaction can result in significant negative and even catastrophic consequences for the aircraft.

The use of a laser to supply energy has been experimentally shown to be a good approach for both general and local flow control. Experimental research (Tret'yakov et al., 1994, 1996) shows that an extensive region of energy supply is realized in the supersonic flow when a powerful optical pulsating discharge is applied, with a thermal wake developing behind the area where the energy is supplied.

A cone or hemisphere in the thermal wake, located from 1.0 to 4.0 diameters distance from the focal plane of irradiation from a $CO_2$ laser, results in a reduction of aerodynamic drag of over a factor of two when a 100-kHz pulse frequency is applied (Tret'yakov et al., 1996). The thermal wake becomes continuous for 10–100-kHz radiation pulses (Tret'yakov et al., 1996).

Theoretical modeling results of the influence of a heat-release pulsating source on the supersonic flow around a hemisphere are presented by Guvernyuk & Samoilov (1997). The explicit total-variation-diminishing (TVD) method in Chakravarthy's) formulae (Chakravarthy & Osher, 1985; Chakravarthy, 1986) is applied in these calculations (Guvernyuk & Samoilov, 1997). In the case of $M$ =3, $\gamma$ =1.4 and a constant deposited energy per unit mass, the aerodynamic load upon the body exhibited a decrease. A pulse repetition rate corresponded to a minimum drag was determined and it was concluded that the use of the pulsating energy supply might be more effective than a constant energy source.

Other results (Georgievskii & Levin, 1988) show that pulse repetition rate, power supplied to the flow and the area into which this energy is supplied all greatly influence both the pressure distribution and the model surface and its flow regimes.

The energy supply parameters such as intensity and heat spot configuration influence the flow re-formation significantly as their combination determines the possibility of either airflow choking in the source (i.e. with the separated wave) or the choke-free flow. This considerably affects the spot properties behind the flow and consequently the stagnation pressure and configuration resistance.

This work presents the results of numerical simulation of the flow around a hemisphere at both the symmetric and asymmetric energy supply into the flow, when the energy supply is realized at $90^0$ angle to the velocity vector of the incoming supersonic airflow.

The two types of the heat spot form considered were: the axis-symmetric spot (i.e. thin disk in the two-dimensional space) and the heat spot of the ellipsoidal form (in the three-dimensional space) with its main axis perpendicular to the symmetry axis. The results of the numerical simulation correspond well with the experimental data (Adegren et al., 2001).

## 2. Problem definition

Let us consider the energy supply from above the sphere and along the airflow at Mach number $M_\infty$ = 3.45 and ratio of specific heats $\gamma$ = 1.4 in the incoming supersonic gas flow, i.e. the same as in (Adegren et al., 2001). The energy supply scheme is illustrated in Figure 1. Assume that at the time $t$ =0, a pulsating power supply source is initiated in front of the sphere.

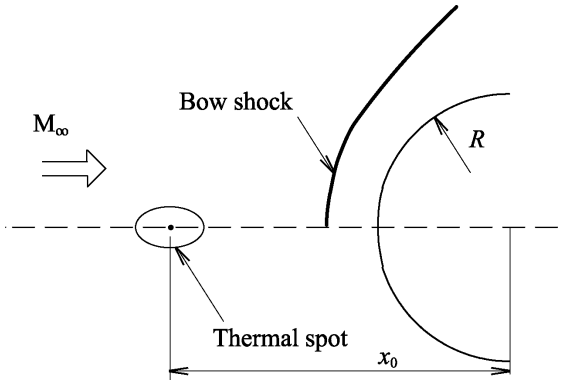


Fig. 1. Schematic of energy supply.

The equations of gas dynamics in the cylindrical coordinates, in contrast to (Bazyma & Rashkovan, 2005) are in the form that includes the azimuthal component

$$\frac{\partial \rho r}{\partial t}+\frac{\partial \rho u r}{\partial x}+\frac{\partial \rho \upsilon r}{\partial r}+\frac{\partial \rho \omega}{\partial \varphi}=0\,; \tag{1}$$

$$\frac{\partial \rho u r}{\partial t}+\frac{\partial (p+\rho u^2) r}{\partial x}+\frac{\partial \rho u \upsilon r}{\partial r}+\frac{\partial \rho u \omega}{\partial \varphi}=0\,; \tag{2}$$

$$\frac{\partial \rho \upsilon r}{\partial t}+\frac{\partial \rho u \upsilon r}{\partial x}+\frac{\partial (p+\rho \upsilon^2) r}{\partial r}+\frac{\partial \rho \upsilon \omega}{\partial \varphi}=p\,; \tag{3}$$

$$\frac{\partial \rho \omega r}{\partial t}+\frac{\partial \rho u \omega r}{\partial x}+\frac{\partial (p+\rho \upsilon^2) r}{\partial r}+\frac{\partial (p+\rho \omega^2)}{\partial \varphi}=0\,; \tag{4}$$

$$\frac{\partial \rho e r}{\partial t}+\frac{\partial \rho u (e+p/\rho) r}{\partial x}+\frac{\partial \rho \upsilon (e+p/\rho) r}{\partial r}+\frac{\partial \rho \omega (e+p/\rho)}{\partial \varphi}=\rho q r\,, \tag{5}$$

where $p$ - pressure; $\rho$ - density; $u$, $\upsilon$, $\omega$ - components of the velocity vector on $x$, $r$ and $\varphi$ respectively; $e$ – total energy of the mass unit of the gas; $q$ – energy supplied to the mass of the gas by the external source; $t$ – time. The system is completed with the perfect gas equation:

$$p=(\gamma-1)\rho e\,. \tag{6}$$

The energy supply is prescribed the same as in (Bazyma & Rashkovan, 2005; Guvernyuk & Samoilov, 1997):

$$q=W(x,r)\sum_{n=1}^{\infty}\frac{1}{f}\delta\left(t-\frac{n}{f}\right), \tag{7}$$

where $\delta$ – is the Dirak's impulse function; $f$ – pulse repetition rate; $W$ – average mass density of the energy supply. Here, in contrast to (Bazyma & Rashkovan, 2005; Guvernyuk & Samoilov, 1997), $W$ was taken in the form that permits modeling different shapes of heat spot at the asymmetric energy supply:

$$W=W_0\left(\frac{p_\infty}{\rho_\infty}\right)^{3/2}\frac{1}{R}\exp\left(-\frac{k_1(r\cos\varphi)^2+k_2(x-x_0)^2+k_3(r\sin\varphi)^2}{L^2}\right), \tag{8}$$

where $W_0$, $k_1$, $k_2$, $k_3$ and $L$ are constants defining deposited energy density and thermal spot shape.

## 3. Numerical method

Similar to (Bazyma & Rashkovan, 2005), the solution of the system of equations (1-4) was conducted using the Godunov´s method (Godunov, 1976). The 110×60 and the 110×60×32

grids were used for the axis-symmetric and the three-dimensional problems respectivelly. In both cases the grid was designed with densening of the nodes near the body or in the areas of energy supply (i.e. the incoming flow disturbance areas).

The calculations were performed using the same finite difference scheme of the first-order approximation as that used by (Godunov, 1976). Computational grid used in calculations is shown in Figure 2.

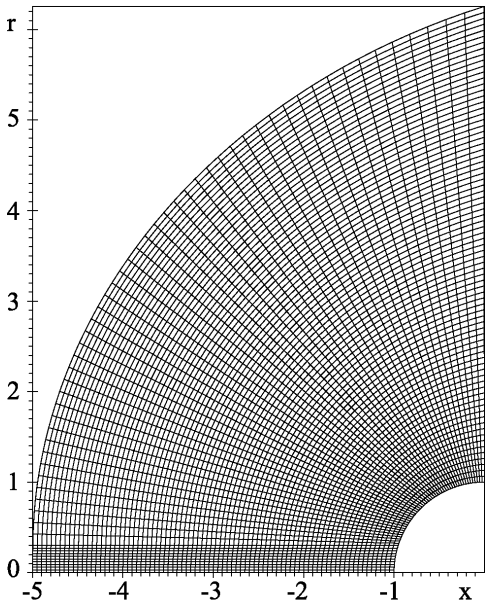


Fig. 2. Computational grid.

The necessary and sufficient condition for stability is that the permissible spacing in time $\tau$ must satisfy the inequality

$$\frac{\tau}{\tau_x}+\frac{\tau}{\tau_y}\le 1 \tag{9}$$

resulting from a stability study of Godunov's difference scheme realized on the system of non-stationary acoustic equations on a uniform rectangular (or parallelogram) grid. Here, $\tau_x$and $\tau_y$ are the time spacing of the one-dimensional scheme. Physically $\tau_x$ and $\tau_y$ are mean time intervals, in which waves appearing at the break decomposition on the cell boundary reach the neighboring boundaries:

$$\tau_x = \frac{\Delta x}{\max\left(u+a, a-u\right)}, \tau_y = \frac{\Delta y}{\max\left(\upsilon+a, a-\upsilon\right)}, \tag{10}$$

where $a$ is the velocity of the sound.

The stability condition so given is extended to the quasi-linear equations of gas dynamics. Calculations show that this condition (9) provides the necessary stability. Nevertheless, this condition is usually used with right-hand side less than one.

In our work, the time step was chosen from cell to cell according to the stability condition as follows:

$$\tau_{n-\frac{1}{2},m-\frac{1}{2}} = \left(\frac{\tau_x \tau_r}{\tau_x + \tau_r}\right)_{n-\frac{1}{2},m-\frac{1}{2}}, \overline{\tau} = \min_{n,m} \tau_{n-\frac{1}{2},m-\frac{1}{2}}, \tag{11}$$

In "$k$" space its value with respect to time is calculated using the spacing "$k$+1" as:

$$\tau^{k+1} = K\overline{\tau}^{k}, \tag{12}$$

where $K$ is a safety factor similar in meaning to the Courant number.

In order to use dimensionless values, we make use of the following equalities:

$$\begin{gathered} r = \overline{r}R, \quad x = \overline{x}R, \quad t = \overline{t}R / a_\infty, \quad f = \overline{f}a_\infty / R, \quad a = \overline{a}a_\infty, \\ u = \overline{u}a_\infty, \quad \upsilon = \overline{\upsilon}a_\infty, \quad \omega = \overline{\omega}a_\infty \quad \rho = \overline{\rho}\rho_\infty, \quad p = \overline{p}\rho_\infty a_\infty^2, \quad W = \overline{W}a_\infty^3 / R, \end{gathered} \tag{13}$$

where $a_\infty$ the velocity of the sound of the incident flow. In the following text, we have omitted bars above the dimensionless values $r$, $x$, $t$, $f$, $a$, $u$, $\upsilon$, $\rho$, $p$, $W$.

The boundary conditions are defined similar to those in (Guvernyuk & Samoilov, 1997). On the surface of the body and along the symmetry axis, solid-wall inviscid boundary conditions were applied. Along the external inflow boundary, undisturbed freestream conditions were utilized. On the downstream outflow boundary, extrapolation of the flow quantities from the adjacent internal boundary was performed.

The initial data in calculations without energy deposition corresponded to the dimensionless parameters of the incident stream:

$$p = p_\infty = 1/\gamma, \ \rho = \rho_\infty = 1, \ u = u_\infty = \mathrm{M}_\infty, \ \upsilon = 0, \ \omega = 0, \tag{14}$$

where $\gamma$ is the ratio of specific heats.

Subsequent solutions of the flow field about a hemisphere with energy deposition were initialized using the flow field about a hemisphere solution without energy deposition. The solutions were advanced in time until the average flow conditions were stabilized.

Preliminary supersonic flow calculations around the hemisphere were conducted in (Bazyma & Rashkovan, 2005) to confirm the adequacy of our numerical scheme (see Fig. 3). Data reported in (Guvernyuk & Samoilov, 1997), where the explicit TVD method of

Chakravarthy's formulation (Chakravarthy & Osher, 1985; Chakravarthy, 1986) was used, showed good correspondence in all the observed flow regimes.

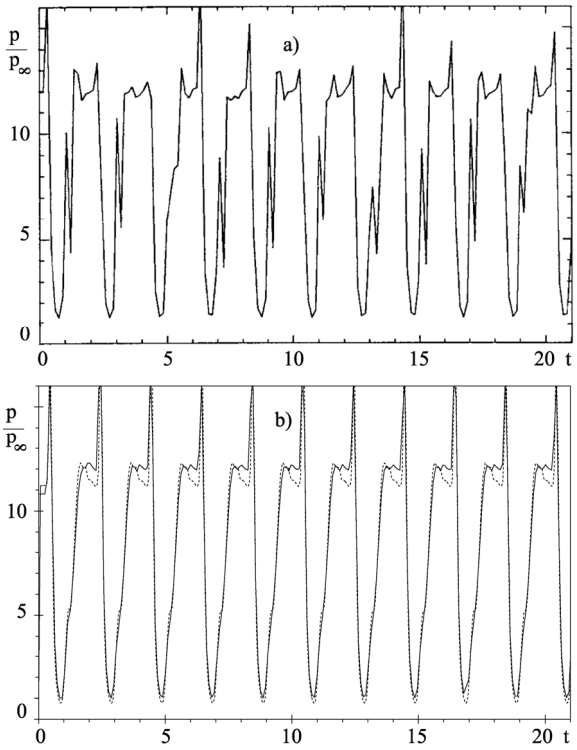


Fig. 3. Pressure at the hemisphere stagnation point versus dimensionless time at the pulse repetition rate $f$=0.5 (spherical heat spot; $W_0$ =20, $x_0$ = -3.5, $L$ = 0.5): a) results of (Guvernyuk & Samoilov, 1997); b) results of (Bazyma & Rashkovan, 2005) (—— – 110×60 grid; - - - - – 219×119 grid).

Shown in Figure 3 is the dependence of the pressure at the stagnation point while flowing around the hemisphere (for $M_\infty$ = 3, $\gamma$ = 1.4) on the dimensionless time at pulse repetition rate $f$ = 0.5. Results are shown both from (Guvernyuk & Samoilov, 1997) (a) and from the our previous work (b). As can be seen from Figure 3, the main pulsation parameters (i.e. period and amplitude) and their character obtained in our work correspond well with the data of (Guvernyuk & Samoilov, 1997). However, while the resolution of the numerical scheme used in (Guvernyuk & Samoilov, 1997) is somewhat higher the scheme used in our previous work (Bazyma & Rashkovan, 2005) allows simulation of the quasi-stationary pulsation process.

Shown in Figure 4a is the flow visualization near the hemisphere under the influence of the pulsating thermal source (spherical heat spot; $W_0$ =20, $x_0$ = -3.5, $L$ = 0.5). These results were obtained in (Guvernyuk & Samoilov, 1997), and compared with the analogous data of the (Bazyma & Rashkovan, 2005) (Figure 4b). As can be seen in Figure 4, bow shock wave

standoff distance, formed recirculation zones and the flow in general reported in (Guvernyuk & Samoilov, 1997) and derived in our work are in good agreement.

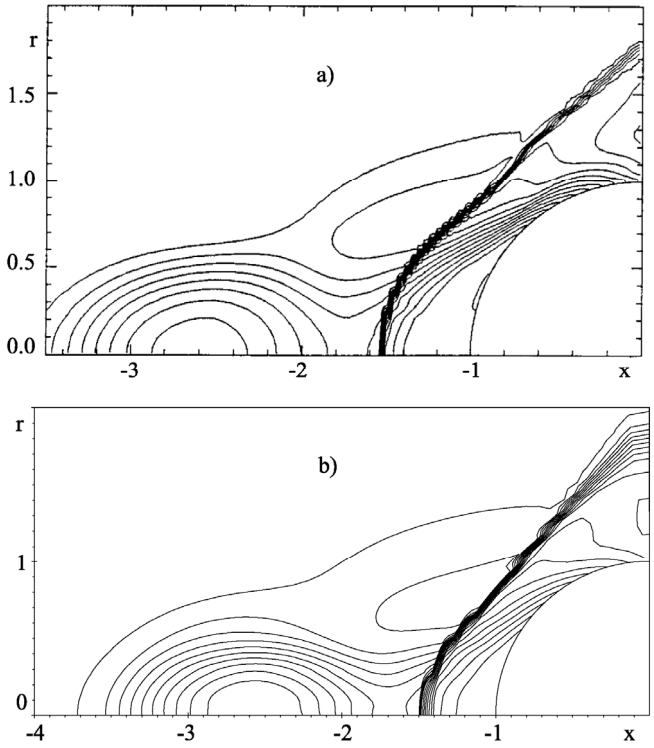


Fig. 4. Mach number isolines while flowing around the hemisphere with supersonic gas flow at pulse repetition rate $f$=2 ($t$=11.2): a) results of (Guvernyuk & Samoilov, 1997); b) results of (Bazyma & Rashkovan, 2005), 110×60 grid.

The grid resolution study was also conducted, with test calculations for hemisphere and cavity hemisphere carried out using the 219×119 grid. The 219×119 grid was obtained through twice the 110×60 grid spacing reduction. Minimum surface cell spacing values were 0.024 for the 110×60 grid (reduced to the sphere radius) and 0.012 for the 219×119 grid.

A comparison of the results derived with the use of the 110×60 (continuous line) and 219×119 grids can be seen in Figure 3b above. As the resolution of the 219×119 (dotted line) grid is higher than that of the 110×60 grid, the solution derived with the use of the 219×119 grid marked out some peculiarities of the pressure change on the compression stage. These peculiarities correspond to the solution in (Guvernyuk & Samoilov, 1997) as well; however they were not seen through the grid applied. It is worth noting that solution difference obtained with the 110×60 and 219×119 grids is rather small for the hemisphere with energy deposition.

The details of the numerical scheme, along with test examples, are given in (Godunov, 1976) and (Bazyma & Kholyavko, 1996; Bazyma & Rashkovan, 2006).

## 4. Results and discussion

When calculating the three-dimensional problem, the energy supply modeled was at $90^0$ angle to the velocity vector of the incoming flow. The two types of the heat spot form considered were: the axis-symmetric spot (i.e. thin disk) and the heat spot of the ellipsoidal form with the main axis perpendicular to the symmetry axis.

The dimensionless parameters of the undisturbed contrary flow are assumed as the initial data in calculations without power supply.

The Table 1 shows the list of operational parameters for the facility used in the wind tunnel experiments (Adegren et al., 2001). This tunnel is a basic blowdown tunnel with an exhaust into atmospheric pressure.

| | |
|---|---|
| Mach Number | 3.45 |
| Operating Stagnation Pressure | 1.4 MPa |
| Typical Stagnation Temperature | 290 K |
| Mass Flow Rate | 9.8 Kg/s |
| Total Run Time | 1.8 minutes |
| Test Area Cross Section | 15 cm x 15 cm |
| Test Area Length | 30 cm |

Table 1. Operating Parameters for the Rutgers Mach 3.45 Supersonic Wind Tunnel.

### 4.1 General calculation procedure

The energy supplied to the mass unit of gas is prescribed in the form

$$q = \gamma^{-3/2} W_0 \exp\left( -\frac{k_1 (r\cos\varphi)^2 + k_2 (x - x_0)^2 + k_3 (r\sin\varphi)^2}{L^2} \right) t^* \delta(t - t^*) . \qquad (15)$$

Here $x_0$ = -3.0 (the energy is supplied at the distance of one diameter of the sphere from its surface, (Adegren et al., 2001)), $t^* = f^{-1}$ at the pulse frequency $f$ =0.00068 (that corresponds to the frequency 10 Hz, (Adegren et al., 2001)). The form of the heat spot is defined by the parameters $L$, $k_1$, $k_2$, $k_3$. The value $L$ =0.01 is fixed in all the calculations; the values $k_1$, $k_2$, $k_3$ are being variated, that permitted to obtain the heat spot dimensions characteristic for the experiment (Adegren et al., 2001) (the volume of the heat spot is evaluated approximately from 1 to 3 $mm^3$; The sphere radius in the experiment is 12.75 mm). Thus, for example, at $k_1$ = $k_2$ = $k_3$ one can obtain a spherical heat spot.

The parameter $W_0$ is being varied in the range 0.19 – 1.75 that in total with the selection of values $k_1$, $k_2$, $k_3$ provides the change of the energy density in the impulse that is provided in the experiment (Adegren et al., 2001) (13 mJ/pulse/1±0.5$mm^3$, 127 mJ/pulse/1.3±0.7$mm^3$, and 258 mJ/pulse/3±1$mm^3$).

The bow shock stand-off distance for the undisturbed model at Mach 3.45 was calculated and compared to the Lobb (Lobb, 1964) approximation to Van Dyke's (Van Dyke, 2003) shock stand-off model. The model predicted the stand-off distances within 3 percent of the calculated distances. The model for shock stand-off distance is given as

$$\Delta = 0.41D\frac{(\gamma-1)\ \ M_\infty^2+2}{(\gamma+1)\ \ M_\infty^2}, \tag{16}$$

where, $\Delta$ is the stand-off distance, $D$ is the sphere diameter, and $M_\infty$ = 3.45 is the freestream Mach number.

### 4.2 Symmetric energy supply

Naturally, obtaining the heat spot form similar to that used in the experiment (Adegren et al., 2001) for the two-dimensional case is impossible. However, with the heat spot size small compared to the size of the streamlined body (i.e. sphere) and low values of the energy density supplied to the incoming flow obtaining some similarity can be expected. For the spheroidal heat spot form (i.e. its axis of rotation coincides with the axis of rotation of the streamlined body), the character of the pressure change in the critical point of the body is sufficiently close (at the stage of compression and the first phase of expansion) to that obtained in the experiment (Adegren et al., 2001) for the value of energy supplied in the pulse in the order of 13mJ/1mm$^3$ (see Figure 5).

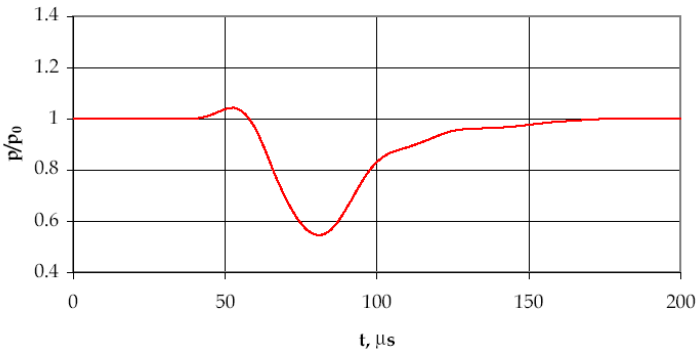


Fig. 5. Pressure variation at the critical point of the sphere versus time: $W_0$ = 0.19, $f$ = 0.00068, ellipsoid heat point; $k_1 = k_3$ = 0.016, $k_2$ =0.39.

Increasing the spot size and the energy supply density will not allow to obtain the conditions fully adequate to those of the physical experiment. At the same time, varying these two parameters (i.e. the size and configuration of the spot on the one hand and the energy supply density on the other hand) allow the character of the pressure change in the critical point of the body adequate to the experiment by the higher values of the energy supply density (127 mJ/pulse/1.3±0.7mm$^3$, and 258 mJ/pulse/3±1mm$^3$) to be obtained.

Character of pressure variation in the critical point of the sphere versus time for other values of $k_1$, $k_2$, and $k_3$ providing smaller volume of the heat spot (i.e. by the factor of 2 approximately) but twice the energy supply density (i.e. $W_0$= 0.38) is shown in Figure 6, curve 1. It is worth noting that the character of the pressure variation in both cases is similar. Curves 2 and 3 in Figure 6, with a considerable difference in pressure amplitude at the compression stage, are obtained for the form of the heat spot that is the flattened axis-symmetric disk with its radius comparable with the radius of the sphere.

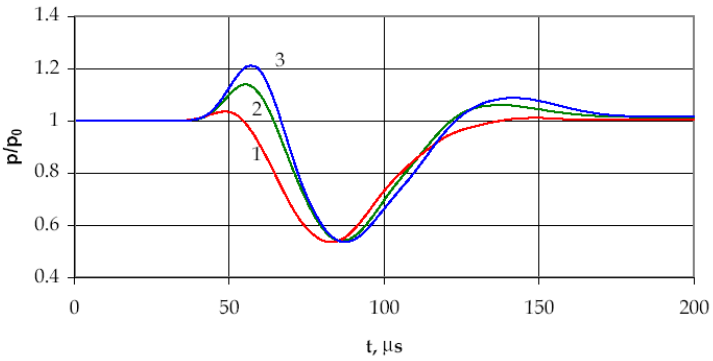


Fig. 6. Pressure variation at the critical point of the sphere versus time: 1 – $W_0$ = 0.38, $f$ = 0.00068, ellipsoid heat point; $k_1 = k_3$ = 0.016, $k_2$ =0.56; 2 – $W_0$ = 0.38, $f$ = 0.00068, disk heat point; $k_1 = k_3$ = 0.00045, $k_2$ =0.089;3 – $W_0$ = 0.38, $f$ = 0.00068, disk heat point; $k_1 = k_3$ = 0.00023, $k_2$ =0.082.

As in the experiment (Adegren et al., 2001; refer figure 20) the time history of recorded pressure at centerline location of sphere surface for the three energy levels shows a common behavior comprised of an initial pressure rise, expansion, compression and transient decay. The expansion, compression and transient decay are similar to the ideal gas Euler simulations of (Georgievskii & Levin, 1993) for the interaction of a thermal spot with a sphere at Mach 3. The expansion lowers the surface pressure at the centerline by 40%. However, the initial compression phase observed in our research and in the experiment (Adegren et al., 2001) was not noted by (Georgievskii & Levin, 1993).

The interaction of the thermal spot, with the bow shock (Figure 7-9, t = 40-90 microseconds) causes a blooming of the bow shock (due to the lens effect of the thermal spot). This behavior is consistent with the simulations of Georgievski and Levin (Georgievskii & Levin, 1993).

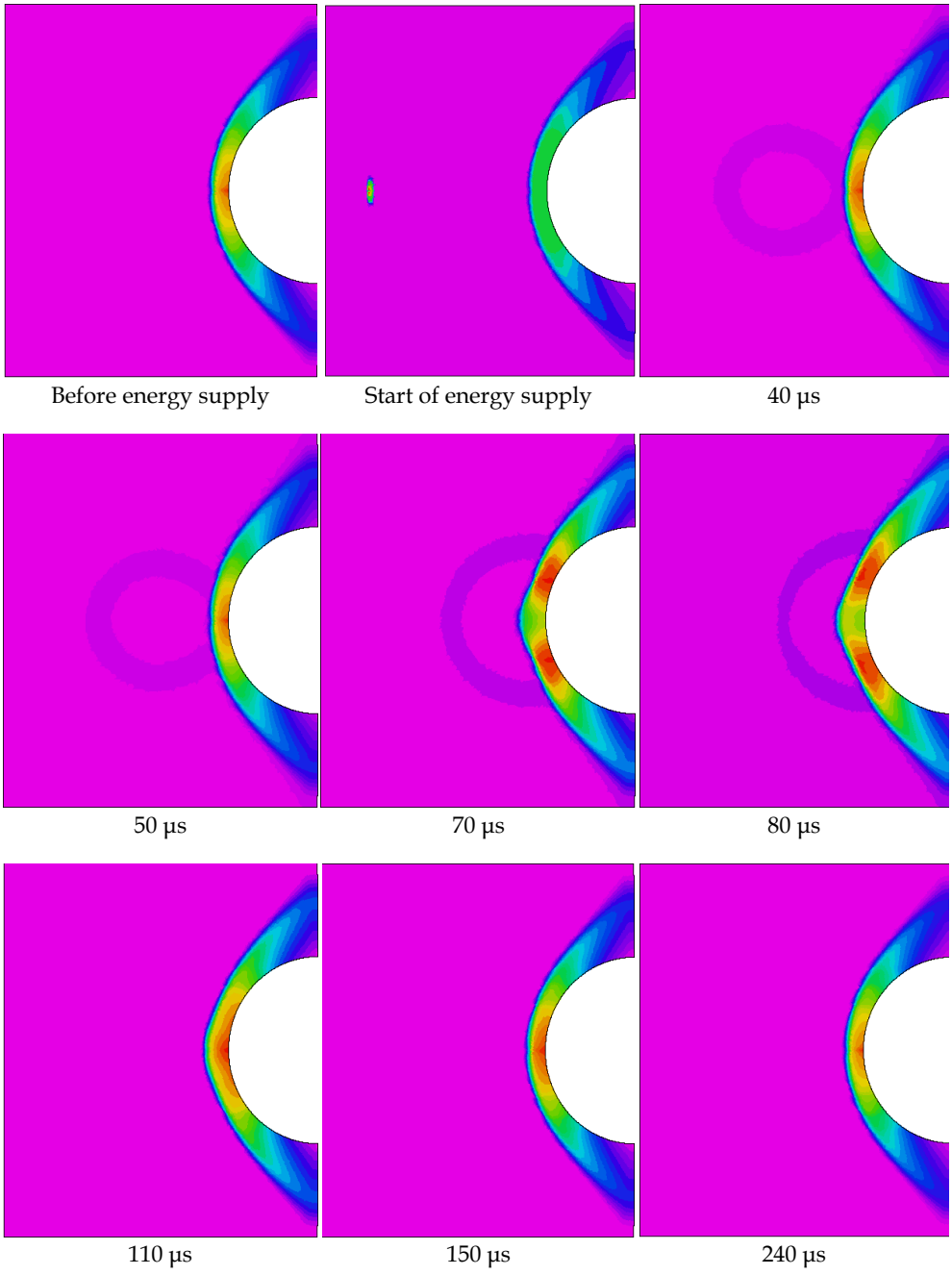


Fig. 7. Time histories of pressure isolines:
$W_0 = 0.38$, $f = 0.00068$, disk heat point; $k_1 = k_3 = 0.00045$, $k_2 = 0.089$.

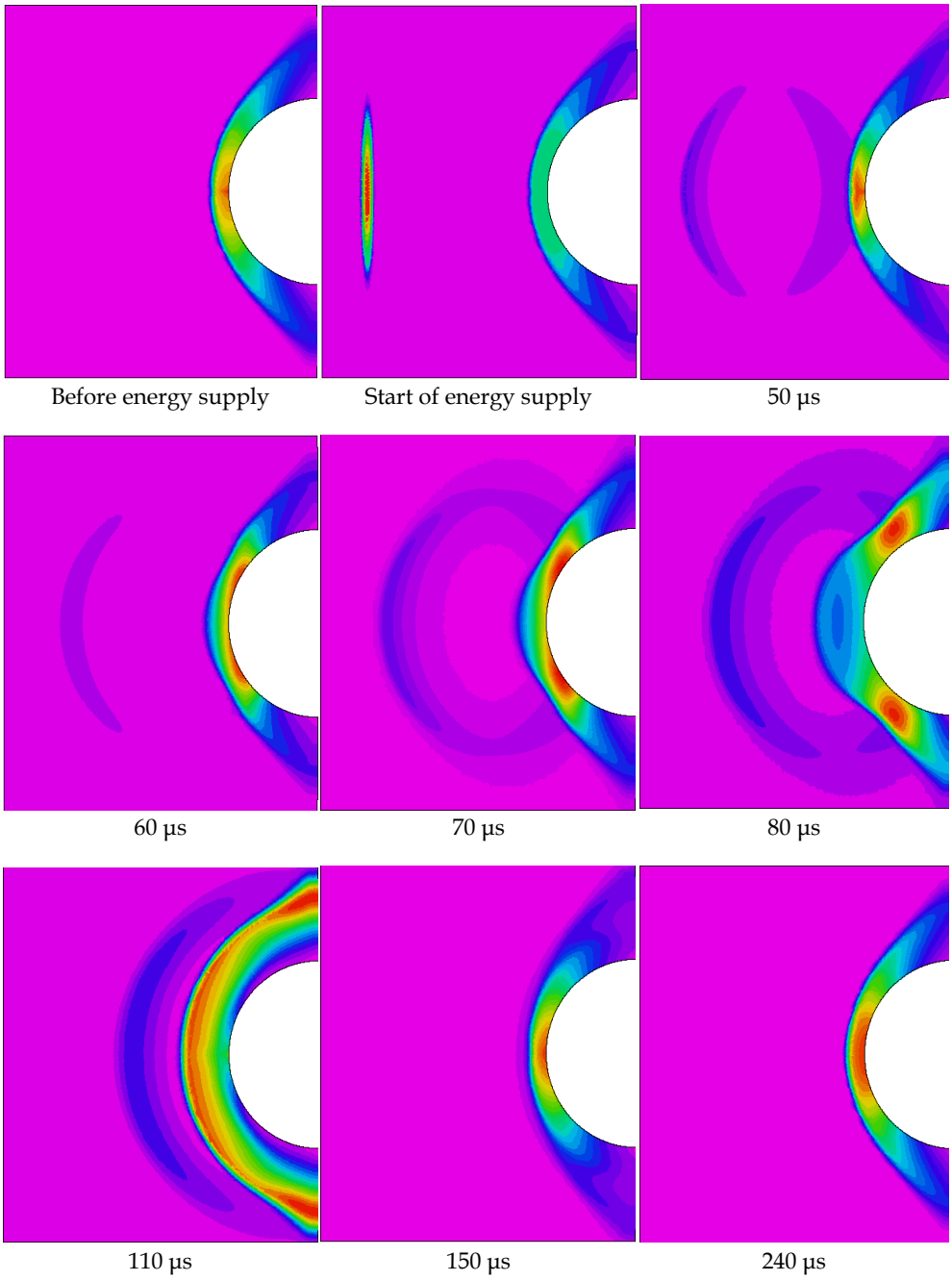


Fig. 8. Time histories of pressure isolines:
$W_0 = 0.38$, $f = 0.00068$, disk heat point; $k_1 = k_3 = 0.00045$, $k_2 = 0.089$.

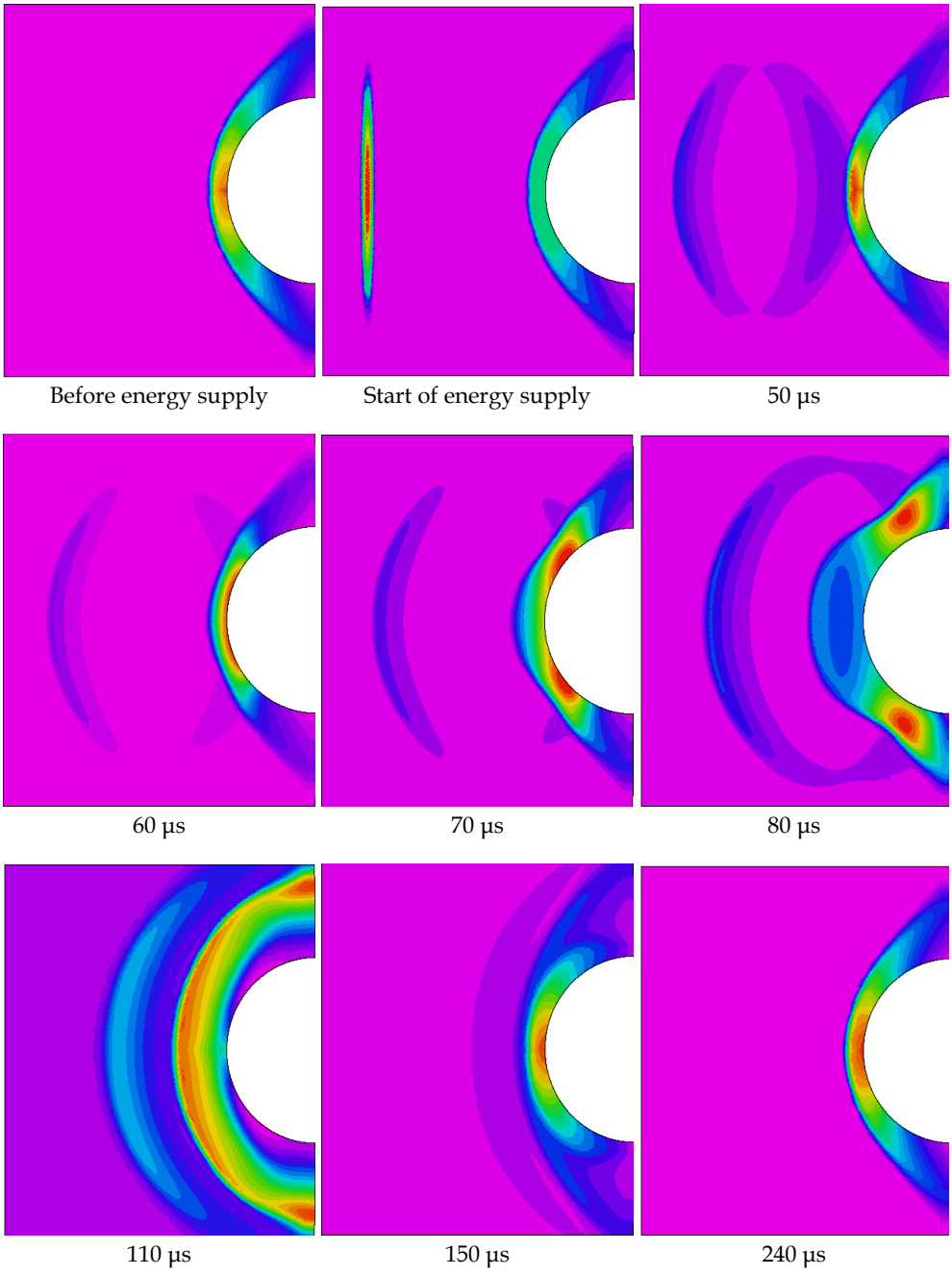


Fig. 9. Time histories of pressure isolines:
$W_0 = 0.38$, $f = 0.00068$, disk heat point; $k_1 = k_3 = 0.00023$, $k_2 = 0.082$.

Naturally, with these conditions satisfied the energy supply density was even less than in the experiment (Adegren et al., 2001). However, the character of the pressure variation at the stage of compression and expansion was similar to that obtained in the experiment for energy supply densities of 127 mJ/pulse/1.3±0.7mm$^3$ and 258 mJ/pulse/3±1mm$^3$.

### 4.3 Asymmetric energy supply

Pressure variation at the critical point of the sphere, relevant to the corresponding pressure obtained before the heat influence, versus time after the energy supply is shown in Figure 10.

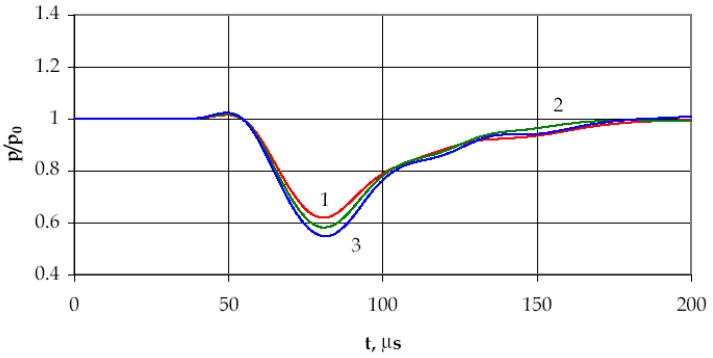


Fig. 10. Pressure variation at the critical point of the sphere versus time:
1 – $W_0$ = 0.5, $f$ = 0.00068, ellipsoid heat point, $k_2 = k_3$ = 0.67, $k_1$ =0.007; 2 – $W_0$ = 1.5, $f$ = 0.00068, ellipsoid heat point, $k_2 = k_3$ = 1, $k_1$ =0.06; 3 – $W_0$ = 1.75, $f$ = 0.00068, ellipsoid heat point, $k_2 = k_3$ = 1, $k_1$ =0.17.

Figure 11 shows the pressure history for the asymmetric energy deposition.

The Mach number in the contrary flow is M=3.45. The distance from the heat spot to the sphere was equal to one diameter of the sphere. The zone of the energy supply was an ellipsoid with the volume in the order of 1mm$^3$ with its rotational axis perpendicular to the incoming flow velocity vector. The process of interaction of the heat track and the sphere contained two stages: short stage of compression and long stage of expansion. The obtained results are in good agreement with the experimental data (Adegren et al., 2001), both quantitatively and qualitatively.

Figure 12 shows the fields of the equal pressure on the sphere surface at 500 μs time after the heat influence (here the pressure is related to the contrary flow pressure). As can be seen, by this time the symmetrical vortex areas on the surface of the sphere still exist. It is worthwhile to point out that the flow rotation velocity is sufficiently high; with its maximum value reaching 0.3 of the contrary flow sound velocity (see Figure 13).

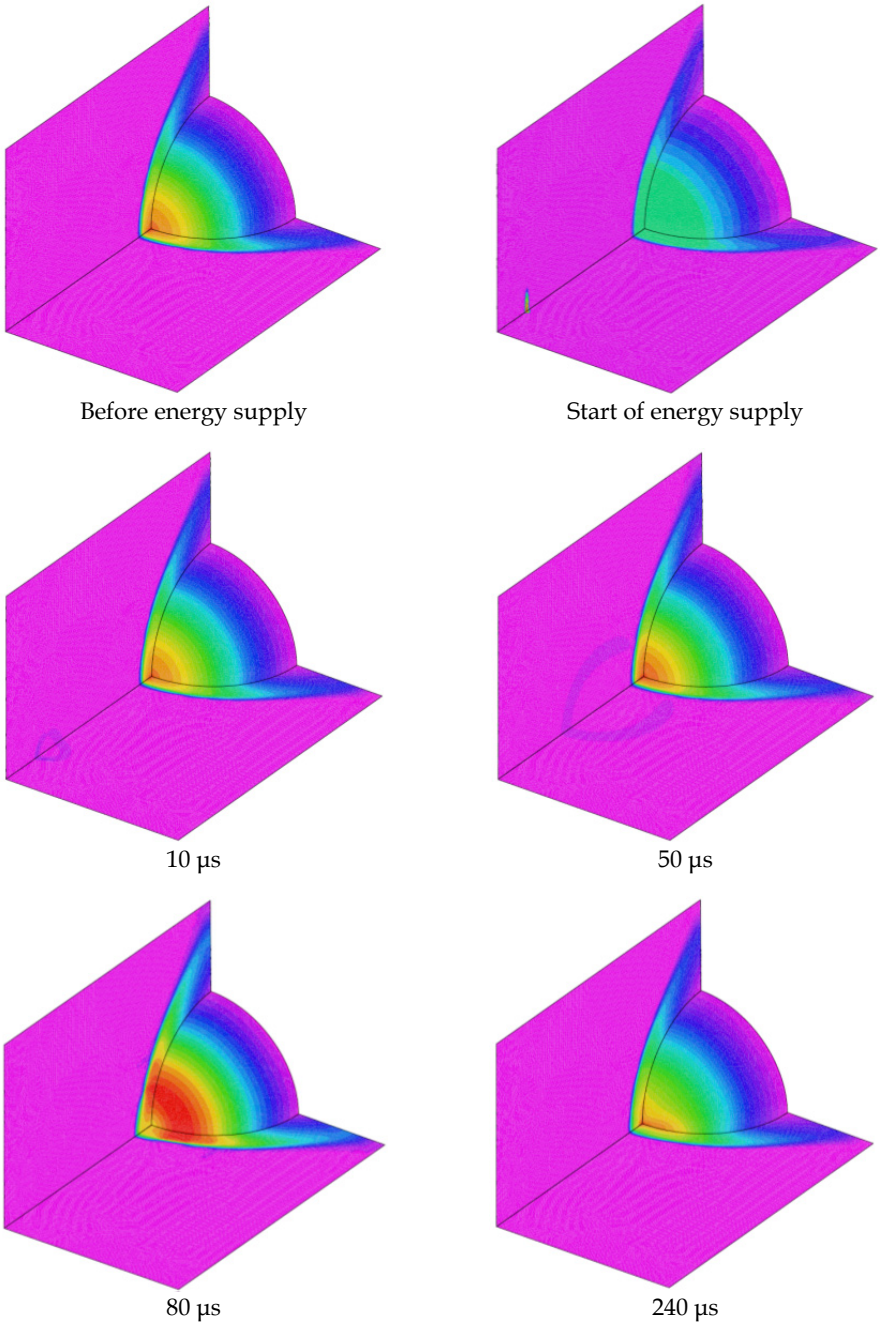


Fig. 11. Time histories of pressure isolines:
$W_0 = 0.5$, $f = 0.00068$, ellipsoid heat point, $k_2 = k_3 = 0.67$, $k_1 = 0.007$.

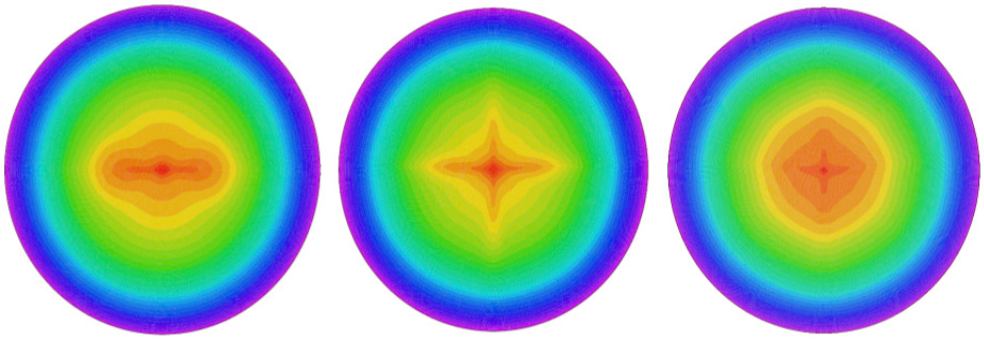

a b c

Fig. 12. Pressure on the sphere surface at 500 μs time after the energy supply:
a - $W_0$ = 0.5, $f$ = 0.00068, ellipsoid heat point, $k_2 = k_3$ = 0.67, $k_1$ =0.007;
b – $W_0$ = 1.5, $f$ = 0.00068, ellipsoid heat point, $k_2 = k_3$ = 1, $k_1$ =0.06;
c - $W_0$ = 1.75, $f$ = 0.00068, ellipsoid heat point, $k_2 = k_3$ = 1, $k_1$ =0.17.

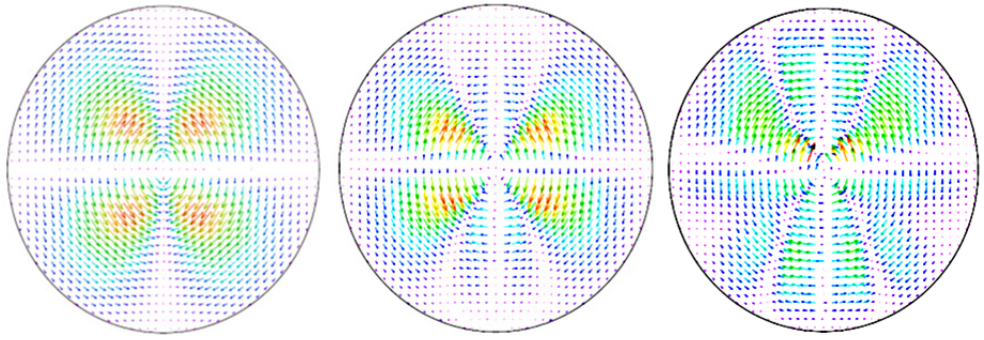

a b c

Fig. 13. The azimuthal velocity component (in the vector form) on the sphere surface at 500 μs time after the energy supply:
a - $W_0$ = 0.5, $f$ = 0.00068, ellipsoid heat point, $k_2 = k_3$ = 0.67, $k_1$ =0.007;
b – $W_0$ = 1.5, $f$ = 0.00068, ellipsoid heat point, $k_2 = k_3$ = 1, $k_1$ =0.06;
c - $W_0$ = 1.75, $f$ = 0.00068, ellipsoid heat point, $k_2 = k_3$ = 1, $k_1$ =0.17.

The energy supply parameters, i.e. the heat spot configuration and the energy supply intensity, influence the flow reconstruction significantly as their combination defines the possibility of either flow choking in the source (i.e. with the separated wave) or the choke-free flow. This considerably affects the track properties behind the flow and consequently the braking pressure and the configuration resistance. Energy supply into the incoming airflow allows the loads caused by the shock-wave influence on the construction elements of aircraft to be minimised.

## 5. Conclusion

The results of our research can be summarized as follows:

- An initial flow compression stage during the lens and blooming interaction process has been observed for both symmetric and asymmetric energy supply conditions;
- A 40% decrease in surface pressure during the 40 microsecond thermal spot interaction time was observed for the case of a sphere in Mach 3.45 flow with varying levels of energy deposition upstream of the bow shock for both symmetric and asymmetric energy supply conditions;
- For the case of symmetric energy supply, the process of heat track and sphere interaction has been found to consist of three stages i.e. an initial compression, expansion, compression and transient decay regardless of the energy input density magnitude;
- For asymmetric energy supply, the process of heat track and sphere interaction has been found to consist of two stages i.e. a short stage of compression followed by a long stage of expansion;
- Thermal spot shape and intensity of energy supply influence reorganization of flow, with their combination affecting properties of the track and stagnation pressure in both symmetric and asymmetric energy supply cases.

The application of energy deposition for local flow control requires low power in terms of the energy deposition into the flow. This low power requirement could potentially translate into small, low weight energy generation systems utilizing optical lasers or electric arc units etc. for effective and efficient flow control. This warrants consideration of the use of energy supply as effective means for solution of local issues of supersonic flow of various aircraft.

## 6. Acknowledgment

The authors would like to express their gratitude to Professor Alexander V. Gaydachuk of the National Aerospace University "Kharkov Aviation Institute" for his input and guidance during the manuscript preparation.

## 7. References

Adegren, R.; Elliot, G.; Knight D.; Zheltovodov, A. & Beutner, T. (2001). Energy deposition in supersonic flows, *AIAA Paper* N2001–0885, 2001

Adelgren, R.; Yan, H.; Elliott, G.; Knight D.; Beutner, T. & Zheltovodov, A. (2005). Control on Edney IV Interaction by Pulsed Laser Energy Deposition, *AIAA J.*, Vol. 43, No. 2, pp. 256-269, ISSN 0001-1452

Bazyma, L. & Rashkovan, V. (2005). Stabilization of Blunt Nose Cavity Flows Using Energy Deposition. *Journal of Spacecraft and Rockets*, Vol.42, No.5, (September-October 2005), pp. 790-794, ISSN 0022-4650

Bazyma, L. & Kholyavko V.I. (1996). A modification of Godunov's finite difference scheme on a mobile grid. *Computational Mathematics and Mathematical Physics*, Vol. 36, No.4, pp. 525-532, ISSN 0965-5425

Bazyma, L. & Rashkovan, V. (2006). Separation Flow Control by the Gas Injection Contrary Supersonic Stream, *AIAA J.*, Vol. 44, No. 12, pp. 2887-2895, ISSN 0001-1452

Chakravarthy, S. & Osher, S. (1985). New Class of High Accuracy TVD Schemes for Hyperbolic Conservation Laws, AIAA Paper 85-0363

Chakravarthy, S. (1986). The Versality and Reliability of Euler Solvers Based on High-Accuracy TVD Formulations," AIAA Paper 86-0243

Georgievskii, P. & Levin, B. (1988). Supersonic Flow Around Bodies in the Presence of External Heat Pulsed Sources, *Technical Physics Letters*, Vol. 14, No. 8, pp. 684–687 (ISSN 1063-7850)

Georgievski, P. & Levin, V. (1993). Unsteady Interaction of a Sphere with Atmospheric Temperature In homogeneity at Supersonic Speed, *Akademiya Nauk SSSR, Izvestiya, Mekhanika Zhidkosti i Gaza*, No. 4, June, pp. 174-183, ISSN 0568-5281

Godunov, S. Ed(s). (1976). *Numerical Solution of Multidimensional Problems in Gas Dynamics*, Nauka, Moscow (in Russian)

Guvernyuk, S. & Samoilov, A. (1997). Control of supersonic flow around bodies by means of a pulsed heat source. *Technical Physics Letters*, Vol.23, No.5, pp. 333-336, ISSN 1063-7850

Lobb, R.K. (1964). Experimental Measurement of Shock Detachment Distance on Spheres Fired in Air at Hypervelocities, In *The High Temperature Aspects of Hypersonic Flow*, Nelson, WC (ed.), pp. 519-527, Pergamon Press, New York, NY

Tret'yakov, P.; Grachev, G.; Ivanchenko, A.; Krainev, V.; Ponomarenko, A. & Tishenko, V. (1994). Optical breakdown stabilization in the supersonic argon flow. *Physics-Doclady*, Vol.39, No.6, pp. 415-416, ISSN 1063-7753

Tret'yakov, P.; Garanin, A.; Grachev, G.; Krainev, V.; Ponomarenko, A.; Tishenko, V. & Yakovlev, V. (1996). Control of supersonic flow around bodies by means of high-power recurrent optical breakdown. *Physics-Doclady*, Vol.41, No.11, pp. 566-567, ISSN 1063-7753

Van Dyke, M.D. (2003). The Supersonic Blunt-Body Problem - Review and Extension. *AIAA J.*, Vol. 41, No. 7, pp. 265-276, ISSN 0001-1452